HHS Public Access

Author manuscript

Mol Pharm. Author manuscript; available in PMC 2020 May 06.

Published in final edited form as:

Mol Pharm. 2019 May 06; 16(5): 1958–1970. doi:10.1021/acs.molpharmaceut.8b01319.

Fenofibrate-Loaded Biodegradable Nanoparticles for the Treatment of Experimental Diabetic Retinopathy and Neovascular Age-Related Macular Degeneration

Fangfang Qiu[†,‡], **Tuo Meng**[Δ], **Qian Chen**[†,§], **Kelu Zhou**[†], **Yan Shao**[†,¶], **Greg Matlock**[†], **Xiang Ma**[†], **Wenjing Wu**[†], **Yanhong Du**[†], **Xiang Wang**[⊥], **Guotao Deng**[†,‖], **Jian-xing Ma**[*,†], and **Qingguo Xu**[*,Δ,#]

[†] Department of Physiology, The University of Oklahoma Health Sciences Center, Oklahoma City, Oklahoma 73104, USA

[‡] Department of Medicine, Section of Endocrinology and Diabetes, The University of Oklahoma Health Sciences Center, Oklahoma City, Oklahoma 73104, USA

[Δ] Department of Pharmaceutics, Virginia Commonwealth University, Richmond, VA 23298, USA

[§] Eye Institute of Xiamen University, Xiamen, Fujian 361000, China

[¶] Tianjin Medical University Eye Hospital, Tianjin 300384, China

[⊥] Department of Cell Biology, The University of Oklahoma Health Sciences Center, Oklahoma City, Oklahoma 73104, USA

[‖] State Key Laboratory of Ophthalmology, Zhongshan Ophthalmic Center, Sun Yat-sen University, Guangzhou, Guangdong 510060, China

[#] Department of Ophthalmology, and Massey Cancer Center, Virginia Commonwealth University, Richmond, VA 23298, USA

Abstract

Fenofibrate is a peroxisome proliferator-activated receptor α (PPARα) agonist and has been shown to have therapeutic effects on diabetic retinopathy (DR). However, the effects of fenofibrate through systemic administration are not as potent as desired due to inefficient drug delivery to the retina. The present study aimed to explore the sustained therapeutic effects of fenofibrate-loaded biodegradable nanoparticles (NP) on both DR and neovascular age-related macular degeneration (AMD). Fenofibrate was successfully encapsulated into poly(lactic-co-glycolic acid) (PLGA) NP (Feno-NP), and Feno-NP were optimized by varying polymer composition to achieve high drug loading and prolonged drug release. The Feno-NP made of PLGA 34kDa demonstrated a drug content of 6% w/w and a sustained drug release up to 60 days *in vitro*. Feno-NP (PLGA 34kDa) was selected for following *in vivo* studies, and one single intravitreal (IVT) injection of Feno-NP into rat eyes with a 30G fine needle maintained sustained fenofibric acid drug level in the eye for more than 60 days. The efficacy of Feno-NP in DR and neovascular AMD was investigated using streptozotocin (STZ)-induced diabetic rats, laser-induced choroidal neovascularization (CNV) rats

[*]Address correspondence to Jian-xing-Ma@ouhsc.edu and qxu@vcu.edu.

and very low-density lipoprotein receptor knockout (*Vldlr*$^{-/-}$) mice. Therapeutic effects of Feno-NP were evaluated by measuring electroretinogram (ERG), retinal vascular leakage, leukostasis, CNV size, and retinal levels of vascular endothelial growth factor (VEGF) and intracellular adhesion molecule-1 (ICAM-1). In diabetic rats, Feno-NP ameliorated retinal dysfunctions, reduced retinal vascular leakage, inhibited retinal leukostasis, and downregulated the overexpression of VEGF and ICAM-1 at 8 weeks after one IVT injection. In addition, Feno-NP reduced retinal vascular leakage and CNV formation in both CNV rats and *Vldlr*$^{-/-}$ mice. Moreover, no toxicity of Feno-NP or Blank-NP to retinal structure and function was detected. Feno-NP exhibited good physiochemical characteristics and controlled drug release profile, conferring prolonged beneficial effects on DR and neovascular AMD.

Keywords

nanoparticle; PLGA; ocular neovascularization; age-related macular degeneration; diabetic retinopathy; PPARα

INTRODUCTION

Retinal neovascularization (RNV) and choroid neovascularization (CNV) are associated with a wide range of ocular diseases such as DR, neovascular AMD, retinopathy of prematurity, and central and branch retina vein occlusion. Among these diseases, DR is the leading cause of vision loss in the working age population [1], while neovascular AMD is the leading cause of visual impairment in the elderly population in industrialized countries [2]. Vascular leakage (hyper-permeability) and neovascularization (NV) are the common features of these diseases and the major causes of visual impairment. Laser photocoagulation, photodynamic therapy, and surgical interventions are important options for neovascular diseases previously; however, these treatments are often associated with unwanted vision-damaging side effects [1–2]. Because VEGF plays a key role in the pathological NV, anti-VEGF agents such as bevacizumab, ranibizumab, pegaptanib, and aflibercept have emerged as current drugs for treating RNV and CNV [1, 3]. However, the anti-VEGF drugs are not always effective for all patients. Approximately half of the patients do not show improved vision after the anti-VEGF therapy, and approximately 10% of patients do not respond at all to the treatment [4]. Anti-VEGF drugs are also not effective for the neuronal cell death, another pathological change in AMD and DR [5]. Moreover, VEGF functions as a retinal neurotrophic factor and its blockade under retinal stress conditions may accelerate retinal cell death [6]. In addition, they are associated with high costs and potential systemic risks such as stroke and thromboembolic events [7–8]. They are also associated with short duration of efficacy and require repetitive IVT injections to maintain the therapeutic effects [3, 9–10]. The frequent visits and injections are difficult for DR and AMD patients, and the risks of retinal detachment and endophthalmitis will increase with the IVT injection frequency [11]. Therefore, novel safe agents and drug delivery system that can achieve long-term effects on these diseases and benefit patients have received great attention.

Fenofibrate, a prodrug of fenofibric acid, is a widely prescribed drug to treat dyslipidemia in clinic [12]. Fenofibrate as a PPARα agonist, has also displayed anti-angiogenic and anti-

inflammatory activities [13–14]. Fenofibrate may offer some advantages over anti-VEGF agents, such as low-cost, fewer side effects and neuroprotective effects [15–16]. In clinical trials, it displayed beneficial effects on DR in type 2 diabetic patients, independent of its effect on dyslipidemia [17–18]. Moreover, our lab [19–20] and others [21] demonstrated that systemic administration of fenofibrate has robust therapeutic effects on DR and neovascular AMD in animal models. However, fenofibrate has a short half-life with the elimination time ~20 h in the blood after oral administration [22], requiring daily systemic dosing. The levels of fenofibrate in the retina, like other drugs, are low after oral administration because of the blood-retina barrier. No fenofibrate or fenofibric acid was detected in Brown Norway rats' eyes following oral administration of fenofibrate [23]. In order to achieve therapeutic fenofibrate level in posterior ocular segment, high oral doses up to 200 mg/60kg/day are required for patients, which can lead to high-dose induced side effects such as nephrotoxicity [24]. Furthermore, we have demonstrated that the therapeutic effect of fenofibrate on DR is independent on its systemic effects, and the efficacy can be achieved through IVT injection [19]. However, small molecular weight drugs, including fenofibrate, demonstrated fast clearance from the vitreous through two main routes: the anterior route via aqueous turnover and the posterior route via uveal blood flow [25]. In our previous work, inhibitory effects of fenofibrate on retinal vascular leakage in STZ-induced diabetic rats and in oxygen-induced retinopathy (OIR) rats are transient, lasting for about 4 days after a single IVT injection [19]. AMD and DR are chronic and progressive, requiring long-term treatments [26]. Thus, frequent intraocular injections of fenofibrate are needed for its translational application for these chronic diseases. Moreover, in preclinical studies, fenofibrate has to be formulated with organic solvents (e.g. DMSO), and the frequent IVT injections containing organic solvents are not practical and can cause retinal apoptosis [27] and retinal dysfunction [28].

Polymeric nano- and micro-particles can be administered by injection and provide controlled release of drugs to target tissues at effective levels, which can increase treatment efficacy, decrease associated side effects and reduce dosing frequency. Therefore, biodegradable polymeric particle-based therapies are being evaluated to deliver drugs to the eye by various routes, including IVT injection and subconjunctival injection [29–33]. Poly (lactic-co-glycolic acid) (PLGA) is an FDA approved, biodegradable and biocompatible polymeric biomaterial with excellent ocular safety for ocular use [34]. A PLGA-based IVT injectable formulation of sunitinib malate for the potentially once or twice per year dosing of patients of neovascular AMD is under clinic trial (NCT03249740). In this study, we developed and optimized fenofibrate-loaded PLGA NP (Feno-NP) with high drug loading and sustained drug release profile. The efcfiacy of Feno-NP was evaluated on DR in STZ-induced diabetic rats, and neovascular AMD in laser-induced CNV rats and *Vldlr*$^{-/}$ mice.

EXPERIMENTAL SECTION

Materials.

PLGA (LA:GA ratio 50:50, acid terminated) with Mw of 5, 18, 34 and 54 kDa (PLGA 5kDa, PLGA 18kDa, PLGA 34kDa, PLGA 54kDa) were purchased from Evonik Corporation (Birmingham, AL). Fenofibrate, Tween 80, streptozotocin, Evans blue, FITC-

dextran (2×10^6 molecular mass, fixable), FITC-conjugated concanavalin-A, mouse anti-β-actin antibody and organic solvents were purchased from Sigma-Aldrich (St. Louis, MO). Polyvinyl alcohol (PVA) solution (Mw = 25 kDa with 88% hydrolysis) was purchased from Polysciences (Warrington, PA). Ketamine hydrochloride and xylazine were purchased from Vedco (St. Joseph, MO), and cyclopentolate (1%) was purchased from Wilson (Mustang, OK).

Preparation of Feno-NP.

NP were prepared using an emulsification method, as described previously with some modification [35]. Briefly, 50 mg PLGA with different molecular weight and 10 mg fenofibrate were fully dissolved in 1 mL dichloromethane (DCM). The oil phase was emulsified in 5 mL 1% PVA solution in an ice-water bath using a probe sonicator (VibraCell, Sonics & Materials Inc., Newtown, CT) with a one-eighth inch stepped microtip under 30% amplitude for 2 min. This emulsion was poured into another 40 mL aqueous phase 0.3% PVA solution under magnetic stirring at 700 rpm for at least 3 hours to allow solvent to evaporate. The solvent was further evaporated by placing the solution in a vacuum chamber for 30 min. The final nanoparticle suspensions were filtered through a 0.7 μm GF/F syringe filter to remove any drug crystals before centrifugation at 8,000 ×g for 25 min, and thoroughly washed with DI water. The final Feno-NP were resuspended in ultrapure water, and one drop of the suspension was applied on glass slide to check whether there were drug crystals using an optical microscope. Blank PLGA NP (Blank-NP) were prepared using the same method, and no fenofibrate was dissolved in the DCM solution. The fresh Blank-NP and Feno-NP were directly used for the following animal studies. A small volume (25 μL) of Feno-NP were lyophilized for the measurement of drug loading.

Nanoparticle Physiochemical Characterization.

Particle size, polydispersity index (PDI) and surface charge of Feno-NP were determined using a Zetasizer Nano ZS90 (Malvern Instruments, Southborough, MA). NP were suspended in 10 mM NaCl solution (pH7.2). Nanoparticle morphology was characterized using transmission electron microscope (TEM) (Jeol JEM-1230, JEOL Ltd., Tokyo, Japan).

Drug Loading and In Vitro Drug Release Study.

The 25μL lyophilized Feno-NP was weighed, dissolved in 1 mL acetonitrile (ACN), and the solution was measured by HPLC after filtering through a 0.22 μm PTFE syringe filter. Isocratic separation was performed on a Shimadzu Prominence LC system equipped with a Pursuit 5 C18 column and mobile phase consisting of acetonitrile/water (80/20 v/v) containing 0.1% trifluoroacetic acid (flow rate = 1 mL/min). Column effluent was monitored by UV detection at 285 nm. The fenofibrate concentration was calculated using an established standard curve. The drug loading (DL) and encapsulation efficiency (EE) were calculated as follows:

$$\text{DL (\%)} = \text{(amount of fenofibrate in particles)} / \text{(weight of particles)}$$

EE (%) = (actual fenofibrate loading) / (theoretical fenofibrate loading)

The *in vitro* release profile of fenofibrate was measured using a membrane dialysis method, and 400 μL of the Feno-NP suspension (~4 mg NP) was sealed in a dialysis tubing cellulose membrane (molecular weight cutoff of 14 kDa, Sigma Aldrich). The sealed dialysis membrane was placed into a 50 mL conical tube containing 12 mL of 0.2% tween 80 in PBS (pH 7.4) and incubated at 37°C on a platform shaker (140 rpm). Tween 80 is used to increase the solubility of fenofibrate in the release medium, and the solubility of fenofibrate in the release medium was measured to be 9.4 μg/mL. The entire release media was collected at predetermined intervals and replaced with another 12 mL of fresh 0.2% Tween 80 PBS solution. Sample collection and release medium replacement was carried out at 2h, 4h, 8h, 24h in the first day, daily during the first week, and then every other day throughout the whole 2 months. The release experiments were conducted in triplicate. Fenofibrate concentration in the collected release media was measured by HPLC.

Animals.

Male Brown Norway (8 weeks old, Charles River, Wilmington, MA) and *Vldlr* $^{-/-}$ mice (Jackson Laboratory, Bar Harbor, ME) were used in this study. Care, use, and treatment of the animals were in agree with the ARVO Statement for the Use of Animals in Ophthalmic and Vision Research, and local ethics committee approval was obtained. In all procedures, animals were anesthetized with an intramuscular injection of 50 mg/kg ketamine hydrochloride mixed with 5 mg/kg xylazine, and pupils were dilated with topical administration of 1% cyclopentolate.

Measurement of Fenofibric Acid in Eyecups of Rats.

Five microliters of Feno-NP (30 μg fenofibrate) was injected into the vitreous of Brown Norway rats with a 30G needle. At day 4, 7, 14, 30 and 60 days after the injection, rats were sacrificed and their eyecups containing vitreous, retina, choroid, and sclera, were obtained and stored at −80 °C until assay. Fenofibrate exerts therapeutic effects only after it is converted to fenofibric acid by esterase [36], which exists in plasma and tissues including ocular tissues [37]. In order to detect only active drug levels released from Feno-NP, we measured fenofibric acid in the eyecups using LC-MS/MS as previously reported with some modifications [23]. In brief, the eyecup was homogenized in 300 μL water with a Fasprep96 homogenizer (MP Biomedicals, LLC.). Tissue homogenate was diluted in acetone and an internal standard (ketoprofen) was added, and then centrifuged at 5,000 ×g for 5 min at 4°C. The supernatant was collected and then transferred to a pre-conditioned SPE (Thermofisher). Following the loading of 200 μL of supernatant, the plate was washed with 200 μL of water with EDTA, and 200 μL of methanol. A collection plate was then placed under the SPE plate, and 2 × 75 μL of methanol was used for elution. This eluent was then injected into the LC-MS/MS. Analysis was performed using an API 4000 mass spectrometer (AB Sciex) coupled to a Nexera ×2 UHPLC system (Shimadzu Corporation). Fenofibric acid and ketoprofen were separated using a Thermo Accucore C18 column (50 mm × 2.1 mm). The mobile phase was methanol/H_2O (80:20) containing 0.1% formic acid (flow rate is 0.3 mL/min). The column temperature was maintained at 40°C. The MS detector was operated in

multiple reaction monitoring (MRM) mode at unit mass resolution with a dwell time of 100.0 ms for all test compounds. The optimized mass spectrometric parameters, MRM transitions for fenofibrate and fenofibric acid are m/z 361.0 to 121.0 in positive ESI mode and m/z 319.0 to 232.9 in negative ESI mode, respectively. Data were acquired and analyzed using Analyst software version 1.4 (Applied Biosystems). Mean concentration time curve was used for pharmacokinetics analysis. The peak tissue concentration (C_{max}) and the time to reach C_{max} (T_{max}) were calculated.

Efficacy of Feno-NP on DR in STZ-Induced Diabetic Rats.

Diabetes was induced by STZ injection as described previously [19]. Blood glucose levels were measured 3 days after the STZ injection and monitored weekly thereafter. Only animals with consistently elevated glucose levels >350 mg/dL were considered diabetic. One month after STZ injection, a single IVT injection of 5 μL Blank-NP (0.5 mg NP) or Feno-NP (30 μg fenofibrate) was given. Eight weeks after the IVT injection, the effects of Feno-NP on DR were evaluated by measuring retinal function, retinal vascular leakage, retinal leukostasis, and the expression levels of VEGF and ICAM-1.

Efficacy of Feno-NP on Laser-Induced CNV in Rats.

CNV was induced by laser photocoagulation as described previously [20]. A wavelength of 532 nm, a spot size of 75 μm, an exposure time of 100 ms and a power of 500 mW were applied. Eight spots were applied in each eye. Only burns that generated a bubble, indicating the rapture of Bruch's membrane, were included in the study. A single IVT injection of 5 μL Blank-NP (0.5 mg NP) or Feno-NP (30 μg fenofibrate) was given immediately after laser injury. Vascular leakage and CNV size were measured after two weeks.

Efficacy of Feno-NP on Ocular NV in *Vldlr*$^{-/-}$ Mice.

A single IVT injection of 1.5 μL Blank-NP (150 μg NP) or Feno-NP (9 μg fenofibrate) was given to *Vldlr*$^{-/-}$ mice at age of P21. One month after the injection, vascular leakage was measured, and numbers of subretinal NV (SRNV) and intra-retinal NV (RNV) lesions were counted in choroidal and retinal flat mount, respectively.

Toxicities of Blank-NP and Feno-NP to the Structure and Function of the Retina in Healthy Rats.

A single IVT injection of 5 μL Blank-NP (0.5 mg NP) or Feno-NP (30 μg fenofibrate) was performed in normal rats. Retinal function was examined at 2 weeks and 4 weeks post injection, and retinal structure was examined at 4 weeks post injection.

Electroretinogram (ERG) Recording.

ERG was recorded using a Espion Visual Electrophysiology System (Diagnosys, LLC) as previously described [38]. Briefly, rats were dark adapted overnight, and ERG was elicited by flash stimuli with a Ganzfeld photo-stimulator at intensity of 600 cd.s/m^2. The a- and b-wave amplitudes in both eyes were recorded and analyzed.

Optical Coherence Tomography (OCT).

A SD-OCT device (Bioptigen Inc. Durham. NC, USA) was used to record the retinal thickness [20]. Images were captured with the rectangular scan at 1000 A-scans per B-scan, and 100 B-scans per frame. Total retinal thickness (TRT) was measured perpendicular to the surface of retinal pigment epithelial (RPE) layer and retinal nerve fiber layer (RNFL) at 12, 3, 6, and 9 o'clock positions, 500 μm away from the center of optic nerve head (ONH) using the built-in software (InVivoVU, Bioptigen), and then averaged. The examiners were blinded to the treatment information.

Retinal Vascular Permeability Assay.

Retinal vascular permeability was measured using the Evans blue (30 mg/kg) as a tracer, as described previously [20].

Retinal Vascular Leukostasis Assay.

The adherent leukocytes in the retinal vasculature were stained by perfusion with FITC-conjugated concanavalin-A (200 μg/ml), as described previously [19]. The number of leukocytes adherent in the retinal arteries, veins and their first grade branches in the whole retina was counted.

Western Blot Analysis.

Western blot analysis was performed as described previously [20]. Individual protein bands were semi-quantified by densitometry using ImageJ and normalized by β-actin levels. Rabbit anti-VEGF antibody (Abcam, Cat#ab46154), goat anti-ICAM-1 antibody (Abcam, Cat#ab27536), and mouse anti-β-actin antibody (Sigma-Aldrich, Cat#A5441) were used.

Fundus Photography (FP) and Fundus Fluorescein Angiography (FFA).

FP and FFA were performed as described previously [20]. For CNV rats, images were captured at 1 and 5 min after the i.p. injection of fluorescein solution, and fluorescein leakage was graded (Table 1). For *Vldlr*$^{-/-}$ mice, fluorescein leakage spots were quantified at 5 min after the injection.

Choroidal and Retinal Flat Mount Stained with FITC-Dextran (FITC-D).

As described previously [20], fixable FITC-D (20 mg/mL) was injected into anesthetized animals at a dose of 10 mL/kg through the femoral vein. The animals were sacrificed at 5 mins after FITC-D injection and the eyes were enucleated and fixed in 4% paraformaldehyde for 2 hours. The retina and eyecup were flat-mounted separately on slides, and fluorescent images were captured. NV areas or numbers were measured with the ImageJ software.

Statistical Analysis.

Statistical analysis was performed using SPSS 15.0 software (SPSS, Chicago, IL). Values were expressed as n (%) or mean ± standard error of mean (SEM). Categorical variables were compared using the Chi-square (x^2) test. Quantitative data were analyzed using one or

two-way analysis of variance (ANOVA) followed by Bonferroni post hoc tests. $P < 0.05$ was considered statistically significant.

RESULTS

Characteristics of Feno-NP.

Fenofibrate was successfully encapsulated into PLGA NP with different molecular weight PLGA polymers using the emulsification method. The physicochemical properties of Feno-NP were shown in Table 2. All Feno-NP were monodispersed (PDI <0.1), had particle size around 250 nm and possessed a spherical shape (Figure 1A). Feno-NP exhibited a nearly neutral surface charge, contributed by the PVA coating on NP surface [35]. The PVA coatings can further stabilize feno-NP, prevent particle aggregation, and allow smooth IVT injection of Feno-NP through fine gauge needles. There were no drug crystals in Feno-NP suspensions after filtering and washing. Drug loading in Feno-NP increased with the molecular weight of PLGA (Table 2). Relatively high molecular weight PLGA 34kDa and PLGA 54kDa achieved high drug loading of 6% and 7.9% w/w, respectively, corresponding to an encapsulation efficiency of 36% and 47%. There were also no drug crystals when PLGA 34kDa and PLGA 54kDa were used to formulate Feno-NP. While PLGA 18 kDa and PLGA 5kDa were used, the drug loading was reduced to 4.1% and 1.1%, respectively. We observed plenty of drug crystals in PLGA 18 kDa and PLGA 5kDa Feno-NP before filtering (data not shown), indicating a poor drug encapsulation in NP of lower molecular weight PLGA.

Fenofibrate was released from Feno-NP in a controlled manner under sink conditions *in vitro* (Figure 1B). The drug release rate from Feno-NP was significantly affected by the molecular weight of PLGA. Quick drug release with an obvious burst release was observed when PLGA 5kDa was used for Feno-NP, and 100% of drug was released within 1 week. Feno-NP prepared with PLGA 18kDa and 34kDa demonstrated a long-lasting drug release profile in a controlled manner ranging from 1 month to 2 months, respectively, without obvious initial burst release (Figure 1B). Feno-NP made of PLGA 54kDa only released ~70% of loaded drug by 2 months, demonstrating a slow release lasting much longer than 2 months. The drug release profiles for PLGA 34kDa and PLGA 54kDa appeared to be tri-phasic with a first order release during the first month and a short-period rapid release, followed by another gradual drug release to reach plateau. The rapid release around 1 month could be attributed to the degradation of PLGA 34kDa and PLGA 54kDa in Feno-NP allowing the rapid diffusion of fenofibrate. Based on the drug release profiles and the animal efficacy study timeframe (~2 months), Feno-NP (PLGA 34kDa) were selected for following efficacy and toxicity studies as they provide continuous drug release for approximately 2 months *in vitro*.

Ocular Pharmacokinetics of Feno-NP.

The determination of released drug levels in ocular tissues was carried out in BN rats after an IVT injection of Feno-NP. In order to remove the influence from NP-encapsulated fenofibrate to the released drugs, we measured fenofibric acid, the parent drug after the conversion from released fenofibrate. The fenofibric acid levels in eyecups during 2 months

were measured by LC-MS/MS (Figure 2). The calculated T_{max} was 14 days and C_{max} was 150.5 ng/g, and 0.027% of the total dose was recovered in the eyecup tissue at T_{max}. One single IVT injection of Feno-NP provided sustained levels of fenofibric acid in the eye for at least 60 days, and the fenofibric acid level at 60 days was 33.6 ± 5.1 ng/g.

A Single IVT Injection of Feno-NP Improves Retinal Function in STZ-Induced Diabetic Rats.

Retinal dysfunction, as shown by declined ERG a- and b-wave amplitudes in DR patients and diabetic animals, is one of the signs of DR, and is also the target for DR treatment [39]. Our results demonstrated that both a- and b-wave amplitudes of scotopic ERG were decreased in STZ-induced diabetic rats, compared with non-diabetic rats. IVT Feno-NP partially normalized the ERG decline at both 4 and 8 weeks post injection, compared with diabetic rats without treatment or diabetic rats with IVT injection of Blank-NP (Figure 3). It indicates that IVT Feno-NP has a long-lasting protective effect against the retinal function impairment induced by diabetes for at least 8 weeks. We also observed that NP were still visible in the posterior chamber under fundus photography until 6 weeks (data not shown). However, these diabetic rats developed severe cataract from 2 months after onset of diabetes, subsequently, blocking the visual pathway and preventing further monitoring of NP in the posterior chamber.

A Single IVT Injection of Feno-NP Attenuates Retinal Vascular Leakage and Retinal Edema in STZ-Induced Diabetic Rats.

Retinal vascular leakage is a common pathological feature in DR and a major cause of macular edema and loss of vision in diabetic patients, which can occur or reoccur at any stage of DR. As shown by OCT (Figure 4A, B), the total retinal thickness (TRT) increased in diabetic rats in comparison to normal rats, demonstrating a retinal edema. This result was consistent with the increased retinal vascular permeability in diabetic rats, compared with normal rats (Figure 4C). IVT Feno-NP, but not Blank-NP, prevented the TRT increase in diabetic rats and reduced the retinal vascular permeability at 8 weeks post injection in comparison to diabetic rats without treatment, to a nondiabetic level (Figure 4A-C). It is comparable to the effects achieved via daily oral fenofibrate dosing in our previous study [19]. These results indicate that the single IVT Feno-NP reduces diabetes-induced retinal vascular leakage and retinal edema with a long-lasting effect for at least 8 weeks.

A Single IVT Injection of Feno-NP Reduces Leukostasis in STZ-Induced Diabetic Rats.

Enhanced leukostasis, leukocyte adherence to the retinal vasculature, is another hallmark of DR [40]. Retinal leukostasis is responsible for inducing retinal capillary nonperfusion, endothelium damage and vascular leakage [40]. Our results showed that the number of adherent leukocytes significantly increased in the retinal vasculature of diabetic rats, compared with that in nondiabetic control. Single IVT Feno-NP, but not Blank-NP, significantly decreased the number of adherent leukocytes at 8 weeks after treatment, to a nondiabetic level (Figure 5A, B). The single IVT Feno-NP showed comparable effect to that achieved via daily oral fenofibrate dosing in our previous study [19]. It suggests that IVT Feno-NP has an inhibitory effect on retinal vascular leukostasis.

Feno-NP Attenuate the Overexpression of VEGF and ICAM-1 in the retina of Diabetic Rats.

VEGF and ICAM-1 play important roles in retinal inflammation and vascular leakage in DR [41]. As shown by Western blot analysis, both VEGF and ICAM-1 levels in the retina were elevated in diabetic rats compared with those of non-diabetic rats, while Feno-NP, but not Blank-NP, downregulated the overexpression of these two factors at 8 weeks after the treatment (Figure 6). These results suggest that Feno-NP inhibit the overexpression of VEGF and ICAM-1 in the retinas of diabetic rats.

A Single IVT Injection of Feno-NP Reduces Vascular Leakage and Suppresses the Formation of CNV in Laser-Induced CNV Rats.

We employed laser-induced CNV rats, a commonly used model of CNV with main characteristics of neovascular AMD. The distribution of CNV lesions with different degree of leakage was evaluated by FFA (Figure 7A). It showed that the incidence of Grade 3 lesions, clinically significant CNV lesions, were significantly decreased in the Feno-NP group, but not in the Blank-NP group, compared with the untreated control group. The incidence of Grade 3 was decreased about 70% in the Feno-NP group, compared with the Blank-NP group, similar to the effect of fenofibric acid solution via i.p. injection daily [20]. This result suggests that Feno-NP has an inhibitory effect on vascular leakage from laser-induced CNV in rats. For the evaluation of anti-angiogenic effects of Feno-NP, the CNV area was measured in choroidal flat mounts following angiography with FITC-D. Feno-NP, but not Blank-NP, decreased CNV area compared with that in the group without treatment (Figure 7B, C). The CNV area was decreased about 43% in Feno-NP group, compared with the Blank-NP group, similar to the effect of fenofibric acid solution via i.p. injection daily [20]. These results demonstrate that IVT Feno-NP reduces the vascular leakage from CNV and suppresses the formation of CNV in laser-induced CNV rats.

A Single IVT Injection of Feno-NP Reduces Retinal Vascular Leakage and Suppresses the Formation of IRNV and SRNV in Vldlr$^{-/-}$ Mice.

Vldlr$^{-/-}$ mice are a genetic model recapitulating some phenotypes of neovascular AMD such as subretinal NV and intraretinal NV. Feno-NP, but not Blank-NP, significantly reduced the retinal vascular permeability in *Vldlr*$^{-/-}$ mice, compared with *Vldlr*$^{-/-}$ mice without treatment, as shown by permeability assay (Figure 8C). Consistently, FFA showed that Feno-NP, but not Blank-NP, significantly decreased the number of vascular leakage spots in the fundus of *Vldlr*$^{-/-}$ mice (Figure 8A, B). These results indicate that IVT Feno-NP reduces retinal vascular leakage in *Vldlr*$^{-/-}$ mice. Moreover, we evaluated the effect of Feno-NP on the formation of SRNV and IRNV in choroidal and retinal flat mounts following angiography with FITC-D. Numbers of both SRNV and IRNV were decreased significantly in the Feno-NP group, but not in the Blank-NP group, compared with *Vldlr*$^{-/-}$ mice without treatment (Figure 8D, E), suggesting that IVT Feno-NP inhibits the formation of SRNV and IRNV in *Vldlr*$^{-/-}$ mice.

Intraocular Injection of Feno-NP Has no Detectable Toxicities to the Structure and Function of the Retina.

As shown by ERG (Figure 9A, B), there was no significant difference in amplitudes of both scotopic a- or b-waves among untreated normal rats and those treated with Feno-NP and Blank-NP at both 2 weeks and 4 weeks following NP injection, suggesting that neither Feno-NP nor Blank-NP had toxicity to retinal function in normal rats. Structurally, retina appearance was normal and no retinal detachment, hemorrhage, or evidence of fibrosis was observed in the groups treated with Feno-NP or Blank-NP at 4 weeks after injection, as shown by FP (Figure 9E). In FFA, the retinal vasculature in the eyes treated with NP injection was similar to those without NP injection, with no changes in vascular leakage (Figure 9E). Similarly, no difference was observed in total retinal thickness as shown by OCT among normal rats injected with Feno-NP, Blank-NP and without NP injection (Figure 8C, D). Altogether, no severe ocular toxicity was observed during the experimental period after the IVT injection of NPs in rats.

DISCUSSION

PPARα is a nuclear transcription factor for diverse target genes, and regulates many biological processes including vascular function, oxidative stress, and inflammation [42]. Our previous study demonstrated that downregulated PPARα plays a pathological role in diabetic microvascular complications in animal models [43]. We also showed that *Pparα*$^{-/-}$ mice developed more severe laser-induced CNV, compared with wild type mice, indicating that downregulated PPARα promotes the development of CNV [20]. In addition, *Pparα*$^{-/-}$ mice showed increased ischemia-induced retinal cell death in the OIR model in comparison to wild type mice, suggesting the downregulated PPARα plays a pathogenic role in retinal degenerative diseases. PPARα activation has potent anti-inflammatory activities. The activation of NLRP3 inflammasome plays a pivotal role in the development and progression of inflammatory diseases including ocular diseases such as DR, AMD, glaucoma and dry eye [44]. Fenofibrate, a PPARα agonist, improves the endothelial precursor cell function [45] and protects retinas from neuroinflammation via downregulating the activity of NLRP3 [46]. Fenofibrate has potent therapeutic effects on diabetic microvascular complications in patients [17–18], and displays anti-inflammatory and anti-angiogenic activity on DR and neovascular AMD in animal models, through the activation of PPARα [19–20].

Fenofibrate exhibits low oral bioavailability because of its high lipophilicity [47]. In order to enhance the drug solubility and increase the oral bioavailability, attempts were made to formulate fenofibrate nanocrystals [48], and fenofibrate-encapsulated solid lipid NP [49–50]. Polyvinylpyrrolidone, hydroxypropyl-β-cyclodextrin and gelatin were applied to prepare fenofibrate-encapsulated polymeric NP as potential oral formulations to enhance the bioavailability of fenofibrate by increasing the drug dissolution [51]. Fenofibrate-loaded PLGA microparticles were prepared for treating ischemic stroke, and the drug release only lasted for 7 days [52]. None of these formulations would be suitable for IVT administration for treating DR and AMD to provide sustained efficacy up to a few months. Fenofibrate could also be potentially formulated as a drug crystal suspension for IVT injection, but drug suspensions typically exhibit uncontrollable drug dissolution profiles. Here, we

demonstrated that a biodegradable NP platform with high drug loading and sustained release of fenofibrate effectively alleviated choroidal and retinal NV in rats through a single IVT injection, which avoided repeated injections.

The Feno-NP formulations can be further optimized in terms of drug loading and drug release profiles by changing polymer composition and process parameters [53]. When PLGA polymers with the same terminal carboxyl groups and LA:GA ratio, lower molecular weight PLGA (e.g. PLGA 5kDa) are less hydrophobic than higher molecular weight PLGA (e.g. PLGA 54kDa). Thus, more hydrophobic PLGA 54kDa could achieve higher drug loading of 7.9% than the less hydrophobic PLGA5kDa (only 1.1%). Sustained release of fenofibrate from Feno-NP is likely a result of both the gradual degradation of PLGA and diffusion of fenofibrate through the PLGA matrix. The degradation of PLGA is influenced by the degree of polymer crystallinity, which is affected by the LA:GA ratio, and higher content of PGA leads to quicker degradation [54]. An exception is that PLGA(50:50) is amorphous with fast hydration and exhibits the fastest degradation. PLGA with acidic terminal groups demonstrated faster degradation than ester-terminated PLGA. PLGA(50:50) with carboxyl terminal groups can degrade fast, and the nano-sized NP will facilitate water penetration into NP matrix allowing quick hydrolysis. Therefore, we observed a steady drug release profile without a significant lag phase following the initial rapid drug release, unlike typical PLA/PLGA microspheres [54]. Lower molecular weight PLGA 5kDa NP typically degrades quickly and exhibits a fast drug release profile (all drug released within 1 week *in vitro*), and the higher molecular weight PLGA 54kDa NP degrades much slower with sustained drug release lasting for more than 2 months *in vitro*. We can further increase the drug loading and prolong the drug release by increasing the particle size or using more hydrophobic and less degradable PLGA/PLA.

Feno-NP were manufactured with components that are classified as GRAS materials by the FDA for various uses and have a long history of use in pharmaceutical products, including ophthalmic formulations. PLGA is known to form natural metabolites (lactic and glycolic acids) and is eliminated from the body, offering the advantage of safety [34]. However, cytotoxicity is still a potential concern in nanoparticle-mediated drug delivery. In this study, we have evaluated the potential toxicity of Feno-NP and Blank-NP in the retina in normal rats. Analyses of the ERG response, retinal morphology and retinal vasculature indicated that Feno-NP had no detectable side effects on retinal structure and function. The present study suggests that Feno-NP are safe to the normal retina for intraocular administration at the dose used. We noticed an increased trend of permeability in diabetic rats treated with blank-NP, but this increase had no statistical significance. The IVT injection procedure is a known insult to the retina which may cause retinal inflammatory responses, leading to high permeability.

It was reported that up to 50 μm particles can be injected with 27G needles. The 250 nm size of Feno-NP will allow IVT injection in both animals and patients in the future through fine gauge needles (e.g. 30G). The emulsification method used to prepare Feno-NP is a scalable procedure [35, 55], and it will facilitate the large-scale manufacturing. In the future clinical translation, safer solvents (e.g. ethyl acetate and benzyl alcohol) can replace the DCM at the emulsification procedure to manufacture Feno-NP. These PLGA NP were found to be

noninflammatory after IVT administration to healthy rats. Clinic trials demonstrated that the IVT dexamethasone PLGA implant, Ozurdex®, can sustain the release of dexamethasone in the vitreous cavity to provide therapeutic effects up to 6 months in patients with diabetic macular edema, and showed no obvious retinal toxicity caused by PLGA itself even after repeated applications [56]. Our previous study showed that one single IVT injection of plasminogen kringle 5 loaded PLGA NP (K5-NP) decreased CNV area in a laser-induced CNV rat model for up to 2 weeks [57], as well as reduced retinal NV in the ischemia-induced retinal NV rat model for at least 4 weeks [58].

Fenofibrate has potential anti-inflammatory activities, which may contribute to its protective effects against microvascular impairment and neuronal cell death in many diseases [42]. In this study, our results also demonstrated that Feno-NP attributed to its anti-inflammatory effects by reducing the retinal leukostasis, downregulating the overexpression of VEGF and ICAM-1, and attenuating retinal vascular leakage in STZ-induced diabetic rats, consistent with our previous study on free fenofibrate in the OIR rat model and STZ-induced diabetic rat model [19]. In addition, the present study showed a novel finding that Feno-NP rescued retinal dysfunction in STZ-induced diabetic rats, which has not been reported previously. These results suggest that Feno-NP, similar to free fenofibrate, has beneficial effects on DR. Free fenofibrate after IVT dosing, the active drug levels will decline quickly and disappear in less than 1 week [19]. However, compared with fenofibrate free drug, Feno-NP is more clinically important due to the sustained effects lasting for at least 8 weeks after one single injection (30 μg fenofibrate for rats and 9 μg for mice), which provided continuous effective fenofibric acid level in the eye and had the great potential to reduce injection frequency. In order to achieve similar efficacy in the same animal models, a frequent and high systemic dosing for a long period would be required through either daily i.p. injection at ~25 μg/g/day for 2 weeks (5 mg/day per rat and 0.5 mg/day per mouse) [20], or daily oral administration at ~120 μg/g/day for 7 weeks (24 mg/day per rat) [19]. IVT injection of Feno-NP significantly reduced the total dose by ~2000 times and ~40,000 times in comparison to the i.p. and oral route, respectively. Also, the overall effect of Feno-NP in the present study showed a similar efficacy in comparison to fenofibrate administrated systemically in diabetic rats and laser-induced CNV rats. Therefore, the local IVT delivery of Feno-NP has advantages over fenofibrate solution, not only lowering the drug dose of fenofibrate, but also reducing the frequency of more invasive IVT injections, subsequently decreasing the incidence of high-dose fenofibrate induced nephrotoxicity [24] and the risks associated with frequent IVT injections [11]. Feno-NP formulations can be further modified to achieve increased drug release duration ≥6 months. Ultimately, we would expect potentially IVT dosing of patients with AMD and DR only once to twice per year IVT dosing of patients with AMD and DR.

Diabetic stress results in the over-production of inflammatory factors including VEGF and ICAM-1 [41, 59] in the retina. ICAM-1 mediates leukostasis [59], and VEGF increases retinal leukostasis and vascular permeability [60]. Increased retinal vascular leukostasis leads to retinal capillary closure, causing nonperfusion of vessels, damages the retinal endothelium and promotes vascular leakage [40], leading to macular edema and NV which are responsible for vision loss [61]. Our previous study demonstrated that fenofibrate exerts its beneficial effects on DR via activation of PPARα [19]. Therefore, it is possible that fenofibric acid activates PPARα, resulting in the downregulation of VEGF and ICAM-1 expression, which

in turn inhibits retinal leukostasis, decreases retinal microvasculature impairment, reduces vascular leakage, and ultimately protects retinal dysfunction in DR. Although numerous studies have shown retinal vascular leakage or increased vascular permeability in STZ-diabetic rats, actual retinal edema has not been demonstrated in this model. Using OCT, the present study demonstrated the increase of retinal thickness in STZ-diabetic rats, which have been reported only by a few studies [62–63], suggesting retinal edema is present in this model. IVT Feno-NP significantly reduced retinal thickness in diabetic rats to non-diabetic levels. This observation is consistent with reduced retinal vascular leakage and reduced levels of ICAM-1 and VEGF in diabetic retinas, suggesting Feno-NP alleviate diabetic retinal edema. The beneficial effects of Feno-NP in neovascular AMD were also demonstrated by showing that IVT Feno-NP reduced vascular leakage and attenuated the formation of CNV in both laser-induced CNV rat model, a commonly used CNV model, and *Vldlr*$^{-/-}$ mice, a genetic model of intra-retinal and sub-retinal NV. These results are consistent with our previous study of systemic administration of fenofibric acid on neovascular AMD animal models [20]. Taken together, Feno-NP offer an innovative strategy for delivery of fenofibrate by IVT injection, and this delivery system might be a potential therapeutic approach for macular edema and NV in DR and AMD.

Despite the positive efficacy observed, some limitations exist which remain to be addressed in the future studies. The sink conditions do not exist for the local drug delivery in the vitreous chamber, and a more relevant in vitro release experiment set-up is required to reflect the IVT drug delivery environment. We have not performed the PK of free fenofibrate in DMSO solution at the same time and made a comparison PK between free fenofibrate and Feno-NP. Feno-NP retained and released therapeutically relevant amounts of drug for at least 8 weeks in the eye. The effective drug loading of Feno-NP and release kinetics may need to be optimized. Degradation rates of PLGA and accompanying release profiles of drugs can be controlled by the polymer's physicochemical properties, such as molecular weight, hydrophilicity, and the ratio of lactide to glycolide. The drug release from PLGA NPs could be further prolonged by increasing the polymer molecular weight, the lactide ratio, or the particle size. Key next steps in development include pharmacokinetics and safety testing in larger animals, such as rabbits.

In conclusion, Feno-NP have been successfully formulated using the emulsification method, and these conferred sustained therapeutic effects in both DR and neovascular AMD. Feno-NP showed desired physiochemical characteristics and sustained release profiles. A single IVT injection of the Feno-NP displayed promising therapeutic potential for the treatment of DR and neovascular AMD with prolonged drug release and potentially reduced injection frequency. In addition, Feno-NP are safe for administration to the retina. Further studies are warranted to further explore therapeutic applications of Feno-NP in patients with ocular NV including DR and neovascular AMD.

ACKNOWLEDGMENTS

This study was supported by grants from National Institutes of Health (NIH) grants (EY027827, EY018659, EY019309, GM122744), a Juvenile Diabetes Research Foundation Innovative (JDRF) grant (2-SRA-2014–147-Q-R), an Oklahoma Center for the Advancement of Science and Technology (OCAST) grants (HR16–041), and a Ralph E. Powe Junior Faculty Enhancement Award. The funding organization had no role in the design or conduct

of this research. The authors acknowledge Drew Wassel in Charlesson LLC, Oklahoma City, Oklahoma State, for the assistance with LC/MS/MS analysis.

References

1. Cheung N; Mitchell P; Wong TY, Diabetic retinopathy. Lancet 2010, 376 (9735), 124–136. [PubMed: 20580421]
2. Gehrs KM; Anderson DH; Johnson LV; Hageman GS, Age-related macular degeneration--emerging pathogenetic and therapeutic concepts. Ann Med 2006, 38 (7), 450–71. [PubMed: 17101537]
3. Nguyen DH; Luo J; Zhang K; Zhang M, Current therapeutic approaches in neovascular age-related macular degeneration. Discov Med 2013, 15 (85), 343–8. [PubMed: 23819948]
4. Tranos P; Vacalis A; Asteriadis S; Koukoula S; Vachtsevanos A; Perganta G; Georgalas I, Resistance to antivascular endothelial growth factor treatment in age-related macular degeneration. Drug Des Devel Ther 2013, 7, 485–90.
5. Jager RD; Mieler WF; Miller JW, Age-related macular degeneration. New Engl J Med 2008, 358 (24), 2606–2617. [PubMed: 18550876]
6. Nishijima K; Ng YS; Zhong L; Bradley J; Schubert W; Jo N; Akita J; Samuelsson SJ; Robinson GS; Adamis AP; Shima DT, Vascular endothelial growth factor-A is a survival factor for retinal neurons and a critical neuroprotectant during the adaptive response to ischemic injury. Am J Pathol 2007, 171 (1), 53–67. [PubMed: 17591953]
7. Lim LS; Mitchell P; Seddon JM; Holz FG; Wong TY, Age-related macular degeneration. Lancet 2012, 379 (9827), 1728–38. [PubMed: 22559899]
8. Tolentino M, Systemic and ocular safety of intravitreal anti-VEGF therapies for ocular neovascular disease. Surv Ophthalmol 2011, 56 (2), 95–113. [PubMed: 21335144]
9. Rosenfeld PJ; Brown DM; Heier JS; Boyer DS; Kaiser PK; Chung CY; Kim RY; Group MS, Ranibizumab for neovascular age-related macular degeneration. N Engl J Med 2006, 355 (14), 1419–31. [PubMed: 17021318]
10. Bressler NM, Antiangiogenic approaches to age-related macular degeneration today. Ophthalmology 2009, 116 (10 Suppl), S15–23. [PubMed: 19800535]
11. Jonas JB; Spandau UH; Schlichtenbrede F, Short-term complications of intravitreal injections of triamcinolone and bevacizumab. Eye 2008, 22 (4), 590–1. [PubMed: 18292795]
12. Keating GM, Fenofibrate: A Review of its Lipid-Modifying Effects in Dyslipidemia and its Vascular Effects in Type 2 Diabetes Mellitus. Am J Cardiovasc Drugs 2011, 11 (4), 227–247. [PubMed: 21675801]
13. Chen XR; Besson VC; Palmier B; Garcia Y; Plotkine M; Marchand-Leroux C, Neurological recovery-promoting, anti-inflammatory, and anti-oxidative effects afforded by fenofibrate, a PPAR alpha agonist, in traumatic brain injury. J Neurotrauma 2007, 24 (7), 1119–31. [PubMed: 17610352]
14. Varet J; Vincent L; Mirshahi P; Pille JV; Legrand E; Opolon P; Mishal Z; Soria J; Li H; Soria C, Fenofibrate inhibits angiogenesis in vitro and in vivo. Cell Mol Life Sci 2003, 60 (4), 810–9. [PubMed: 12785728]
15. Losey P; Ladds E; Laprais M; Geuvel B; Burns L; Bordet R; Anthony DC, The role of PPAR activation during the systemic response to brain injury. J Neuroinflammation 2015, 12, 99. [PubMed: 25994490]
16. Esmaeili MA; Yadav S; Gupta RK; Waggoner GR; Deloach A; Calingasan NY; Beal MF; Kiaei M, Preferential PPAR-alpha activation reduces neuroinflammation, and blocks neurodegeneration in vivo. Hum Mol Genet 2016, 25 (2), 317–27. [PubMed: 26604138]
17. Keech AC; Mitchell P; Summanen PA; O'Day J; Davis TM; Moffitt MS; Taskinen MR; Simes RJ; Tse D; Williamson E; Merrifield A; Laatikainen LT; d'Emden MC; Crimet DC; O'Connell RL; Colman PG; investigators F. s., Effect of fenofibrate on the need for laser treatment for diabetic retinopathy (FIELD study): a randomised controlled trial. Lancet 2007, 370 (9600), 1687–97. [PubMed: 17988728]
18. Group AS; Group AES; Chew EY; Ambrosius WT; Davis MD; Danis RP; Gangaputra S; Greven CM; Hubbard L; Esser BA; Lovato JF; Perdue LH; Goff DC Jr.; Cushman WC; Ginsberg HN;

Elam MB; Genuth S; Gerstein HC; Schubart U; Fine LJ, Effects of medical therapies on retinopathy progression in type 2 diabetes. N Engl J Med 2010, 363 (3), 233–44. [PubMed: 20587587]

19. Chen Y; Hu Y; Lin M; Jenkins AJ; Keech AC; Mott R; Lyons TJ; Ma JX, Therapeutic effects of PPARalpha agonists on diabetic retinopathy in type 1 diabetes models. Diabetes 2013, 62 (1), 261–72. [PubMed: 23043158]
20. Qiu F; Matlock G; Chen Q; Zhou K; Du Y; Wang X; Ma J-X, Therapeutic Effects of PPARα Agonist on Ocular Neovascularization in Models Recapitulating Neovascular Age-Related Macular Degeneration. Invest Ophthalmol Vis Sci 2017, 58 (12), 5065–5075. [PubMed: 28980001]
21. Gong Y; Shao Z; Fu Z; Edin ML; Sun Y; Liegl RG; Wang Z; Liu C-H; Burnim SB; Meng SS; Lih FB; SanGiovanni JP; Zeldin DC; Hellström A; Smith LEH, Fenofibrate Inhibits Cytochrome P450 Epoxygenase 2C Activity to Suppress Pathological Ocular Angiogenesis. EBioMedicine 2016, 13, 201–211. [PubMed: 27720395]
22. Vlase L; Popa A; Muntean D; Leucuta SE, Pharmacokinetics and comparative bioavailability of two fenofibrate capsule formulations in healthy volunteers. Arzneimittelforschung 2010, 60 (9), 560–3. [PubMed: 21117499]
23. Lu B; Gao Y; Shen W; Zhang Q; Hu Y; Chen Y, Therapeutic Potential of Topical Fenofibrate Eyedrops in Diabetic Retinopathy and AMD Rat Models. J Clin Exp Ophthalmol 2014, 5 (4).
24. Attridge RL; Frei CR; Ryan L; Koeller J; Linn WD, Fenofibrate-associated nephrotoxicity: a review of current evidence. Am J Health Syst Pharm 2013, 70 (14), 1219–25. [PubMed: 23820458]
25. Urtti A, Challenges and obstacles of ocular pharmacokinetics and drug delivery. Adv Drug Deliv Rev 2006, 58 (11), 1131–1135. [PubMed: 17097758]
26. Kompella UB; Amrite AC; Pacha Ravi R.; Durazo SA, Nanomedicines for back of the eye drug delivery, gene delivery, and imaging. Prog. Retina Eye Res. 2013, 36 (0), 172–198.
27. Galvao J; Davis B; Tilley M; Normando E; Duchen MR; Cordeiro MF, Unexpected low-dose toxicity of the universal solvent DMSO. FASEB J 2014, 28 (3), 1317–30. [PubMed: 24327606]
28. Tsai TI; Bui BV; Vingrys AJ, Dimethyl sulphoxide dose-response on rat retinal function. Doc Ophthalmol 2009, 119 (3), 199–207. [PubMed: 19763650]
29. Jiang C; Moore MJ; Zhang X; Klassen H; Langer R; Young M, Intravitreal injections of GDNF-loaded biodegradable microspheres are neuroprotective in a rat model of glaucoma. Mol. Vis. 2007, 13 (198–99), 1783–1792. [PubMed: 17960131]
30. Pan Q; Xu Q; Boylan NJ; Lamb NWG; Emmert D; Yang J-C; Tang L; Heflin T; Alwadani S; Eberhart CG; Stark WJ; Hanes J, Corticosteroid-loaded biodegradable nanoparticles for prevention of corneal allograft rejection in rats. J Controlled Release 2015, 201 (0), 32–40.
31. Luo L; Yang J; Oh Y; Hartsock MJ; Xia S; Kim Y-C; Ding Z; Meng T; Eberhart CG; Ensign LM; Thorne JE; Stark WJ; Duh EJ; Xu Q; Hanes J, Controlled release of corticosteroid with biodegradable nanoparticles for treating experimental autoimmune uveitis. J Controlled Release 2019, 296, 68–80.
32. Wang B; Tang Y; Oh Y; Lamb NW; Xia S; Ding Z; Chen B; Suarez MJ; Meng T; Kulkarni V; Eberhart CG; Ensign LM; Stark WJ; Hanes J; Xu Q, Controlled release of dexamethasone sodium phosphate with biodegradable nanoparticles for preventing experimental corneal neovascularization. Nanomedicine: NBM 2019, 17, 119–123.
33. Xu Q; Kambhampati S; Kannan R, Nanotechnology approaches for ocular drug delivery. Middle East Afr. J. Ophthalmol. 2013, 20 (1), 26–37. [PubMed: 23580849]
34. Lee S; Hughes P; Ross A; Robinson M, Biodegradable Implants for Sustained Drug Release in the Eye. Pharm Res 2010, 27 (10), 2043–2053. [PubMed: 20535532]
35. Xu Q; Boylan NJ; Cai S; Miao B; Patel H; Hanes J, Scalable method to produce biodegradable nanoparticles that rapidly penetrate human mucus. J Controlled Release 2013, 170 (2), 279–286.
36. Balfour JA; McTavish D; Heel RC, Fenofibrate. A review of its pharmacodynamic and pharmacokinetic properties and therapeutic use in dyslipidaemia. Drugs 1990, 40 (2), 260–90. [PubMed: 2226216]

37. Heikkinen EM; Del Amo EM; Ranta VP; Urtti A; Vellonen KS; Ruponen M, Esterase activity in porcine and albino rabbit ocular tissues. Eur J Pharm Sci 2018, 123, 106–110. [PubMed: 30030098]

38. Deng G; Moran EP; Cheng R; Matlock G; Zhou K; Moran D; Chen D; Yu Q; Ma JX, Therapeutic Effects of a Novel Agonist of Peroxisome Proliferator-Activated Receptor Alpha for the Treatment of Diabetic Retinopathy. Invest Ophthalmol Vis Sci 2017, 58 (12), 5030–5042. [PubMed: 28979999]

39. Lecleire-Collet A; Audo I; Aout M; Girmens JF; Sofroni R; Erginay A; Le Gargasson JF; Mohand-Said S; Meas T; Guillausseau PJ; Vicaut E; Paques M; Massin P, Evaluation of retinal function and flicker light-induced retinal vascular response in normotensive patients with diabetes without retinopathy. Invest Ophthalmol Vis Sci 2011, 52 (6), 2861–7. [PubMed: 21282578]

40. Chibber R; Ben-Mahmud BM; Chibber S; Kohner EM, Leukocytes in diabetic retinopathy. Current diabetes reviews 2007, 3 (1), 3–14. [PubMed: 18220651]

41. Aiello LP; Avery RL; Arrigg PG; Keyt BA; Jampel HD; Shah ST; Pasquale LR; Thieme H; Iwamoto MA; Park JE; et al., Vascular endothelial growth factor in ocular fluid of patients with diabetic retinopathy and other retinal disorders. N Engl J Med 1994, 331 (22), 1480–7. [PubMed: 7526212]

42. Moran EP; Ma JX, Therapeutic Effects of PPAR alpha on Neuronal Death and Microvascular Impairment. PPAR Res 2015, 2015, 595426.

43. Hu Y; Chen Y; Ding L; He X; Takahashi Y; Gao Y; Shen W; Cheng R; Chen Q; Qi X; Boulton ME; Ma JX, Pathogenic role of diabetes-induced PPAR-alpha down-regulation in microvascular dysfunction. Proc Natl Acad Sci U S A 2013, 110 (38), 15401–6. [PubMed: 24003152]

44. Yerramothu P; Vijay AK; Willcox MDP, Inflammasomes, the eye and anti-inflammasome therapy. Eye (Lond) 2018, 32 (3), 491–505. [PubMed: 29171506]

45. Deng Y; Han X; Yao Z; Sun Y; Yu J; Cai J; Ren G; Jiang G; Han F, PPARalpha Agonist Stimulated Angiogenesis by Improving Endothelial Precursor Cell Function Via a NLRP3 Inflammasome Pathway. Cell Physiol Biochem 2017, 42 (6), 2255–2266. [PubMed: 28817808]

46. Liu Q; Zhang F; Zhang X; Cheng R; Ma JX; Yi J; Li J, Fenofibrate ameliorates diabetic retinopathy by modulating Nrf2 signaling and NLRP3 inflammasome activation. Mol Cell Biochem 2018, 445 (1–2), 105–115. [PubMed: 29264825]

47. Guay DRP, Micronized Fenofibrate: A New Fibric Acid Hypolipidemic Agent. Ann Pharmacother 1999, 33 (10), 1083–1103. [PubMed: 10534222]

48. Patel CM; Chakraborty M; Murthy ZVP, Preparation of fenofibrate nanoparticles by combined stirred media milling and ultrasonication method. Ultrason Sonochem 2014, 21 (3), 1100–1107. [PubMed: 24365225]

49. Patil H; Feng X; Ye X; Majumdar S; Repka MA, Continuous Production of Fenofibrate Solid Lipid Nanoparticles by Hot-Melt Extrusion Technology: a Systematic Study Based on a Quality by Design Approach. AAPS J 2014, 17 (1), 194–205. [PubMed: 25344439]

50. Xia D; Shrestha N; van de Streek J; Mu H; Yang M, Spray drying of fenofibrate loaded nanostructured lipid carriers. Asian J Pharm Sci 2016, 11 (4), 507–515.

51. Yousaf AM; Kim DW; Oh Y-K; Yong CS; Kim JO; Choi H-G, Enhanced oral bioavailability of fenofibrate using polymeric nanoparticulated systems: physicochemical characterization and in vivo investigation. Int J Nanomedicine 2015, 10, 1819–1830. [PubMed: 25784807]

52. Klose D; Laprais M; Leroux V; Siepmann F; Deprez B; Bordet R; Siepmann J, Fenofibrate-loaded PLGA microparticles: Effects on ischemic stroke. Eur J Pharm Sci 2009, 37 (1), 43–52. [PubMed: 19168134]

53. Kumari A; Yadav SK; Yadav SC, Biodegradable polymeric nanoparticles based drug delivery systems. Colloids Surf. B Biointerfaces 2010, 75 (1), 1–18. [PubMed: 19782542]

54. Makadia HK; Siegel SJ, Poly Lactic-co-Glycolic Acid (PLGA) as Biodegradable Controlled Drug Delivery Carrier. Polymers 2011, 3 (3), 1377–1397. [PubMed: 22577513]

55. Ashton S; Song YH; Nolan J; Cadogan E; Murray J; Odedra R; Foster J; Hall PA; Low S; Taylor P; Ellston R; Polanska UM; Wilson J; Howes C; Smith A; Goodwin RJA; Swales JG; Strittmatter N; Takáts Z; Nilsson A; Andren P; Trueman D; Walker M; Reimer CL; Troiano G; Parsons D; De Witt D; Ashford M; Hrkach J; Zale S; Jewsbury PJ; Barry ST, Aurora kinase inhibitor

nanoparticles target tumors with favorable therapeutic index in vivo. Sci Transl Med 2016, 8 (325), 325ra17–325ra17.

56. Boyer DS; Yoon YH; Belfort R Jr; Bandello F; Maturi RK; Augustin AJ; Li X-Y; Cui H; Hashad Y; Whitcup SM, Three-Year, Randomized, Sham-Controlled Trial of Dexamethasone Intravitreal Implant in Patients with Diabetic Macular Edema. Ophthalmology 2014, 121 (10), 1904–1914. [PubMed: 24907062]
57. Jin J; Zhou KK; Park K; Hu Y; Xu X; Zheng Z; Tyagi P; Kompella UB; Ma JX, Anti-inflammatory and Antiangiogenic Effects of Nanoparticle-Mediated Delivery of a Natural Angiogenic Inhibitor. Invest Ophthalmol Vis Sci 2011, 52 (9), 6230–6237. [PubMed: 21357401]
58. Park K; Chen Y; Hu Y; Mayo AS; Kompella UB; Longeras R; Ma JX, Nanoparticle-mediated expression of an angiogenic inhibitor ameliorates ischemia-induced retinal neovascularization and diabetes-induced retinal vascular leakage. Diabetes 2009, 58 (8), 1902–13. [PubMed: 19491211]
59. Miyamoto K; Khosrof S; Bursell SE; Rohan R; Murata T; Clermont AC; Aiello LP; Ogura Y; Adamis AP, Prevention of leukostasis and vascular leakage in streptozotocin-induced diabetic retinopathy via intercellular adhesion molecule-1 inhibition. Proc Natl Acad Sci USA 1999, 96 (19), 10836–10841. [PubMed: 10485912]
60. Joussen AM; Poulaki V; Qin W; Kirchhof B; Mitsiades N; Wiegand SJ; Rudge J; Yancopoulos GD; Adamis AP, Retinal vascular endothelial growth factor induces intercellular adhesion molecule-1 and endothelial nitric oxide synthase expression and initiates early diabetic retinal leukocyte adhesion in vivo. Am J Pathol 2002, 160 (2), 501–9. [PubMed: 11839570]
61. Diabetes C; Complications Trial Research, G.; Nathan DM; Genuth S; Lachin J; Cleary P; Crofford O; Davis M; Rand L; Siebert C, The effect of intensive treatment of diabetes on the development and progression of long-term complications in insulin-dependent diabetes mellitus. N Engl J Med 1993, 329 (14), 977–86. [PubMed: 8366922]
62. Tien T; Muto T; Barrette K; Challyandra L; Roy S, Downregulation of Connexin 43 promotes vascular cell loss and excess permeability associated with the development of vascular lesions in the diabetic retina. Mol Vis 2014, 20, 732–41. [PubMed: 24940027]
63. Clermont A; Chilcote TJ; Kita T; Liu J; Riva P; Sinha S; Feener EP, Plasma kallikrein mediates retinal vascular dysfunction and induces retinal thickening in diabetic rats. Diabetes 2011, 60 (5), 1590–8. [PubMed: 21444925]

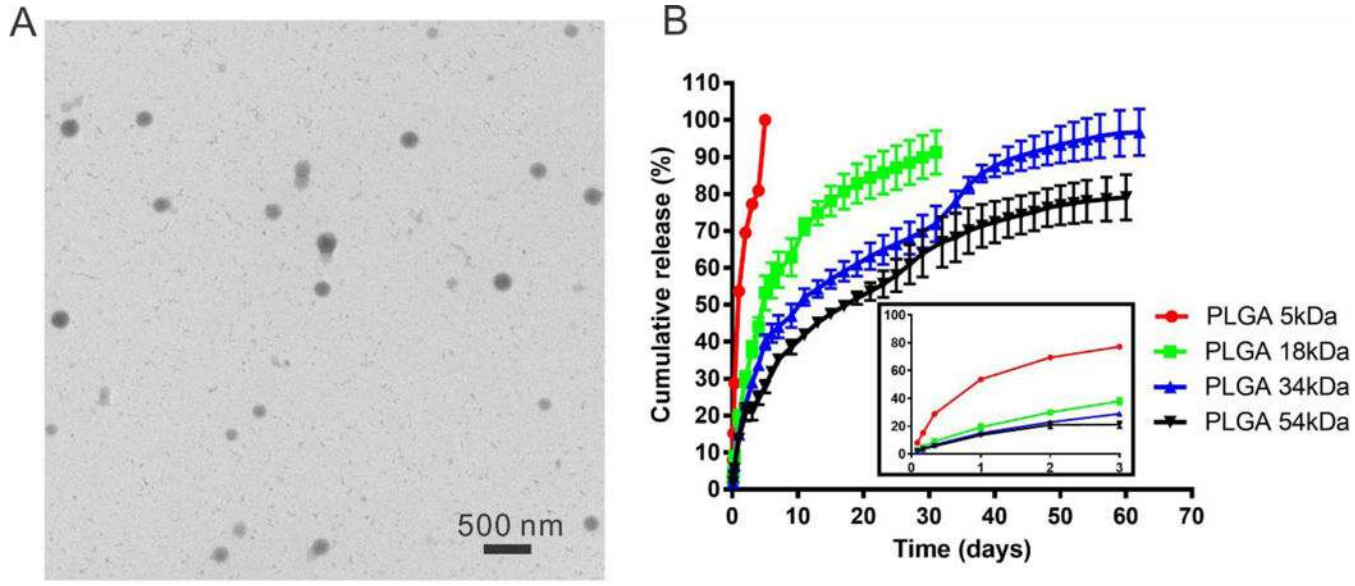

Figure 1.

Characteristics of Feno-NP. (**A**) Representative transmission electron microscope image of Feno-NP (PLGA 34kDa) and (**B**) the *in vitro* drug release profile of Feno-NP made of different polymers. The insert shows expanded drug release profile during the first 3 days.

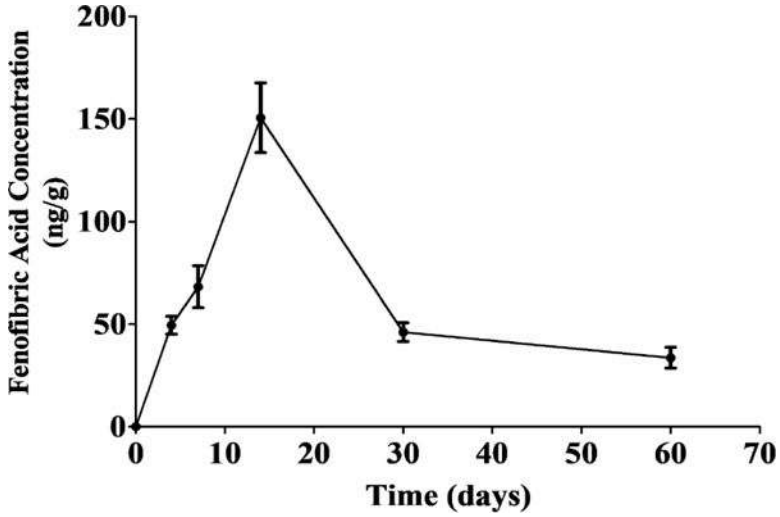

Figure 2.

Pharmacokinetics of Feno-NP in the eyecup tissue containing vitreous, retina, choroid, and sclera. Means ± SEM (n = 4).

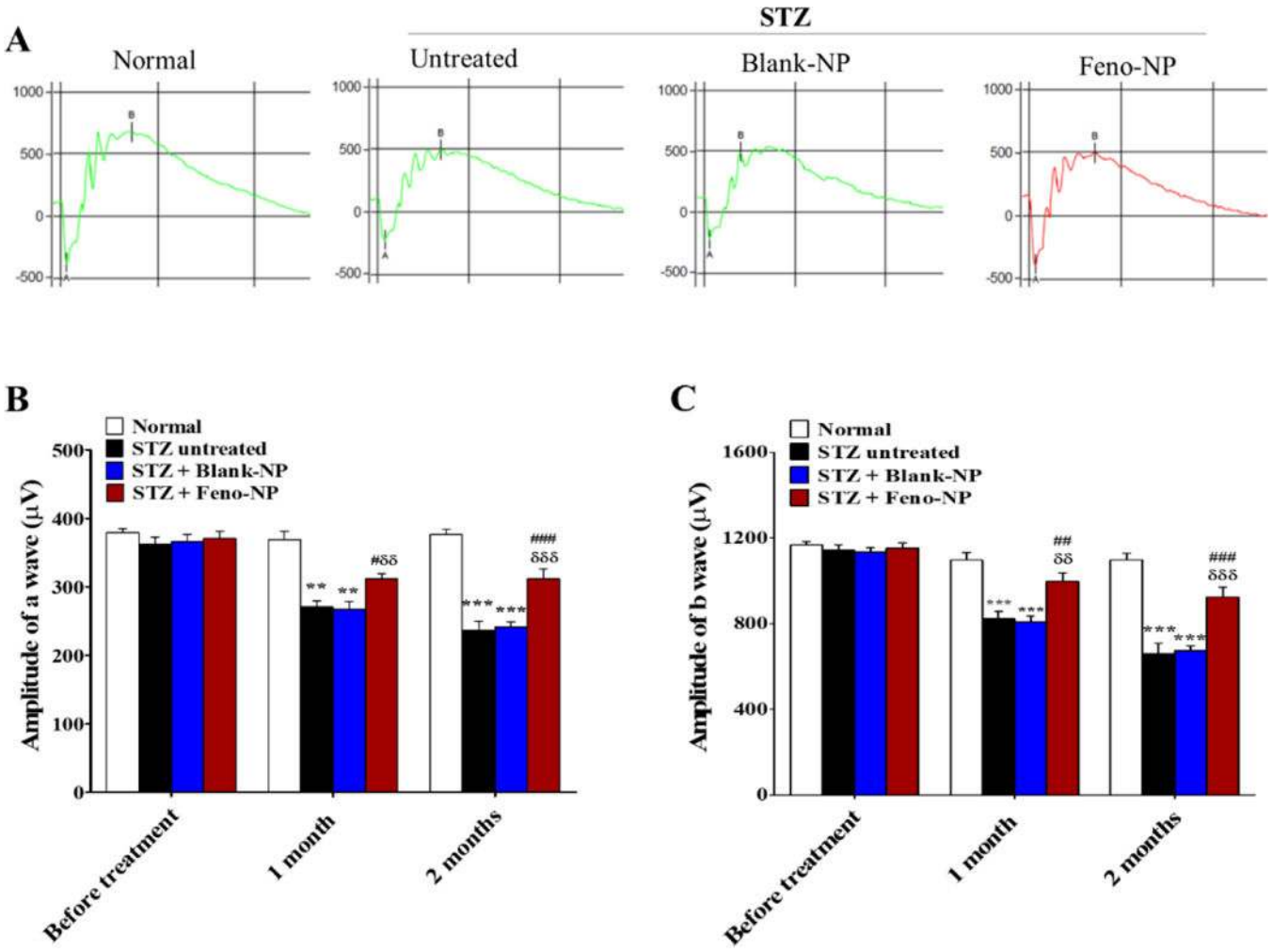

Figure 3.

Effect of Feno-NP on retinal function with ERG in STZ-induced diabetic rats. **(A)** Representative waveforms of ERG in normal rats, untreated diabetic rats, Blank-NP treated diabetic rats, Feno-NP treated diabetic rats. **(B, C)** Quantification of amplitude of a wave (B) and b wave (C) on scotopic ERG. Mean ± SEM (n=10–12/group). Two-way ANOVA followed by Bonferroni post hoc test. ** $P < 0.01$, versus normal rats; *** $P < 0.001$, versus normal rats. # $P < 0.05$, versus untreated diabetic rats; ## $P < 0.01$, versus untreated diabetic rats; ### $P < 0.001$, versus untreated diabetic rats, δδ $P < 0.01$, versus Blank-NP treated diabetic rats; δδδ $P < 0.001$, versus Blank-NP treated diabetic rats.

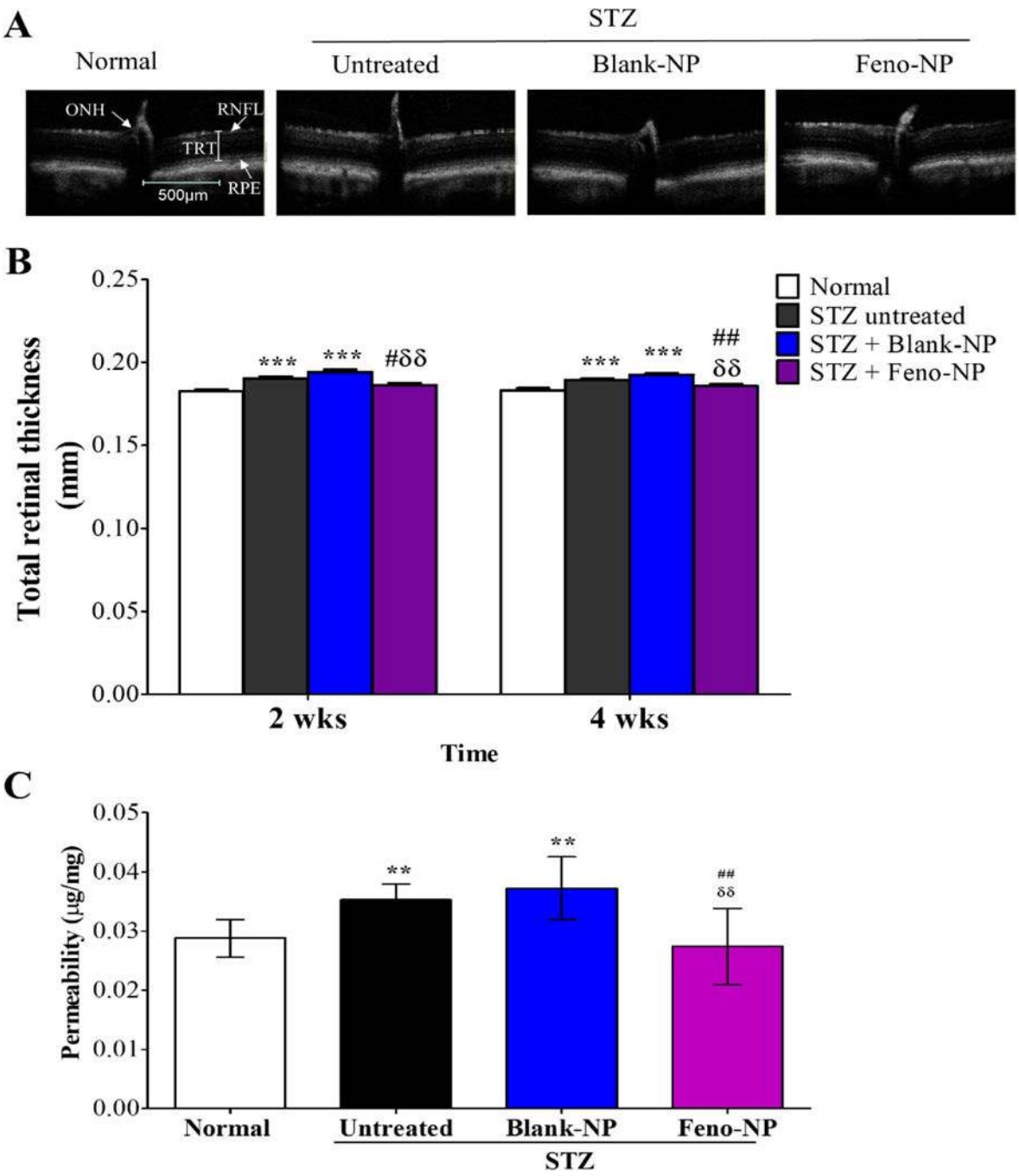

Figure 4.

Effect of Feno-NP on retinal vascular leakage and retinal edema in STZ-induced diabetic rats. Retinal edema was evaluated by total retinal thickness using OCT 2 and 4 weeks after Feno-NP treatment, and retinal vascular leakage was measured by permeability assay 8 weeks after Feno-NP treatment. (**A)** Representative images of OCT; **(B)** Quantification of total retinal thickness (n=12/group) on OCT; **(C)** Quantification of permeability (n=12/group). TRT: total retinal thicknesses; RPE: retinal pigment epithelial layer; RNFL: retinal nerve fiber layer; ONH: optic nerve head. Mean ± SEM. Two-way ANOVA followed by

Bonferroni post hoc test. ** P < 0.01, versus normal rats; *** P < 0.001, versus normal rats. ## P < 0.01, versus untreated diabetic rats. δδ P < 0.01, versus Blank-NP treated diabetic rats.

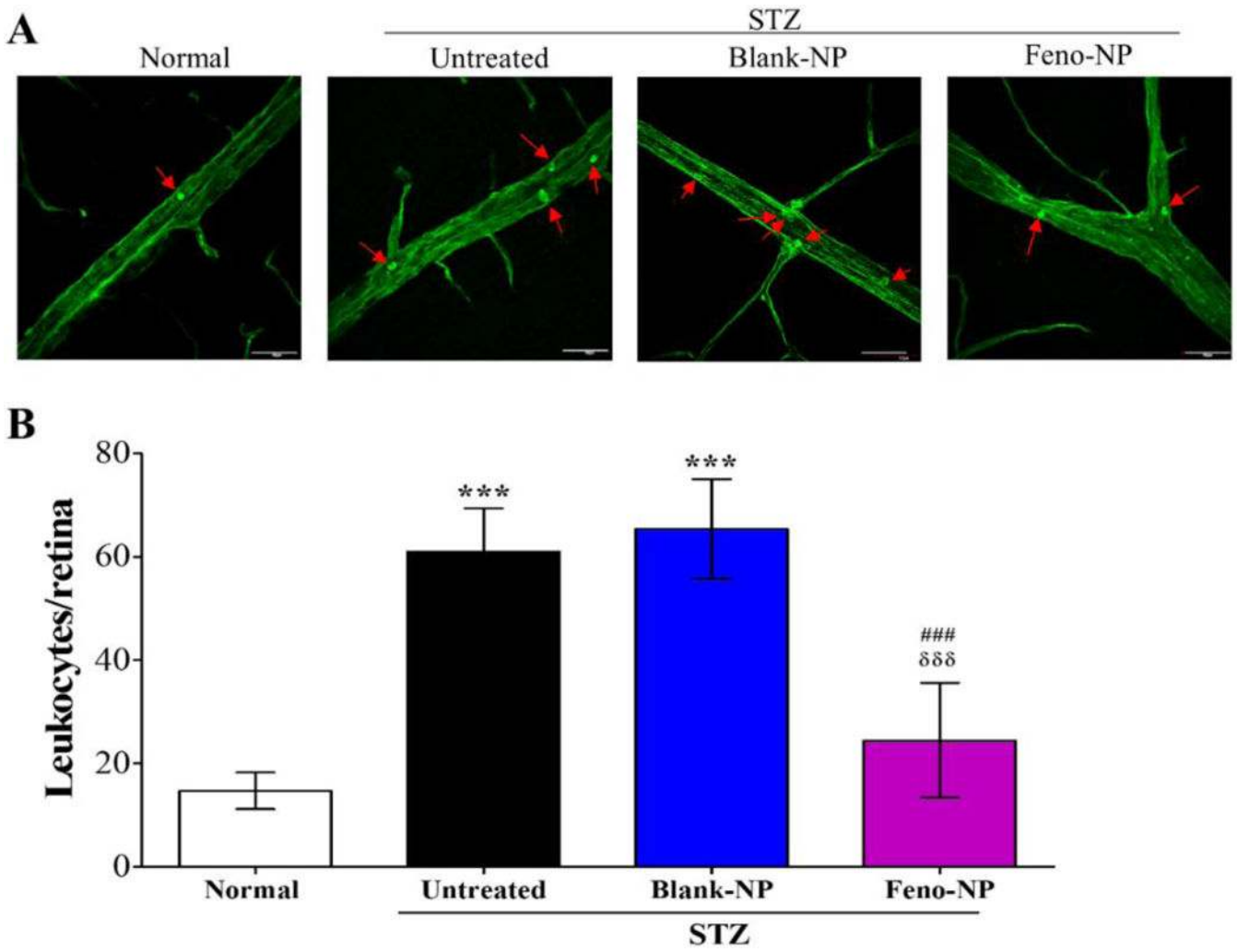

Figure 5.

Effect of Feno-NP on retinal vascular leukostasis in STZ-induced diabetic rats. **(A)** Representative images of retinal vascular leukostasis. Arrows indicated adherent leukocytes. Scale bar: 50 μm. **(B)** Quantification of leukocytes adherent to retinal vasculature 8 weeks after Feno-NP treatment. Mean ± SEM (n = 7/group). Two-way ANOVA followed by Bonferroni post hoc test. *** $P < 0.001$, versus normal rats. ### $P < 0.001$, versus untreated diabetic rats. δδδ $P < 0.001$, versus Blank-NP treated diabetic rats.

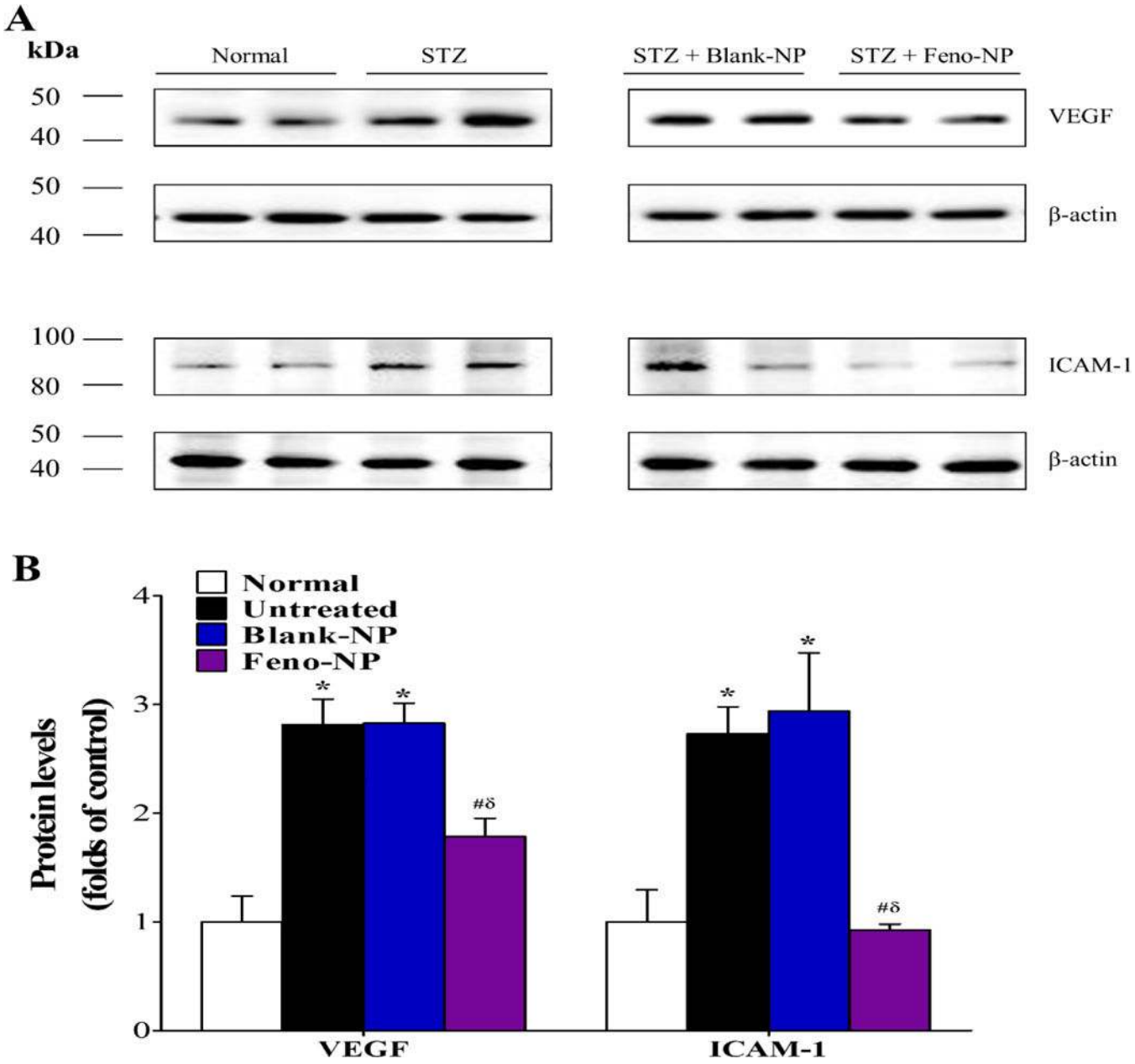

Figure 6.

Effect of Feno-NP on the overexpression of VEGF and ICAM-1 in the retinas of STZ-induced diabetic rat. The retinas were dissected for Western blot analysis 8 weeks after Feno-NP treatment. **(A)** Representative images of VEGF and ICAM-1 blots. **(B)** Quantification data of Western blot analysis. Mean ± SEM (n = 3/group). Two-way ANOVA followed by Bonferroni post hoc test. * $P < 0.05$, versus normal rats. # $P < 0.05$, versus untreated diabetic rats. δ $P < 0.05$, versus Blank-NP treated diabetic rats.

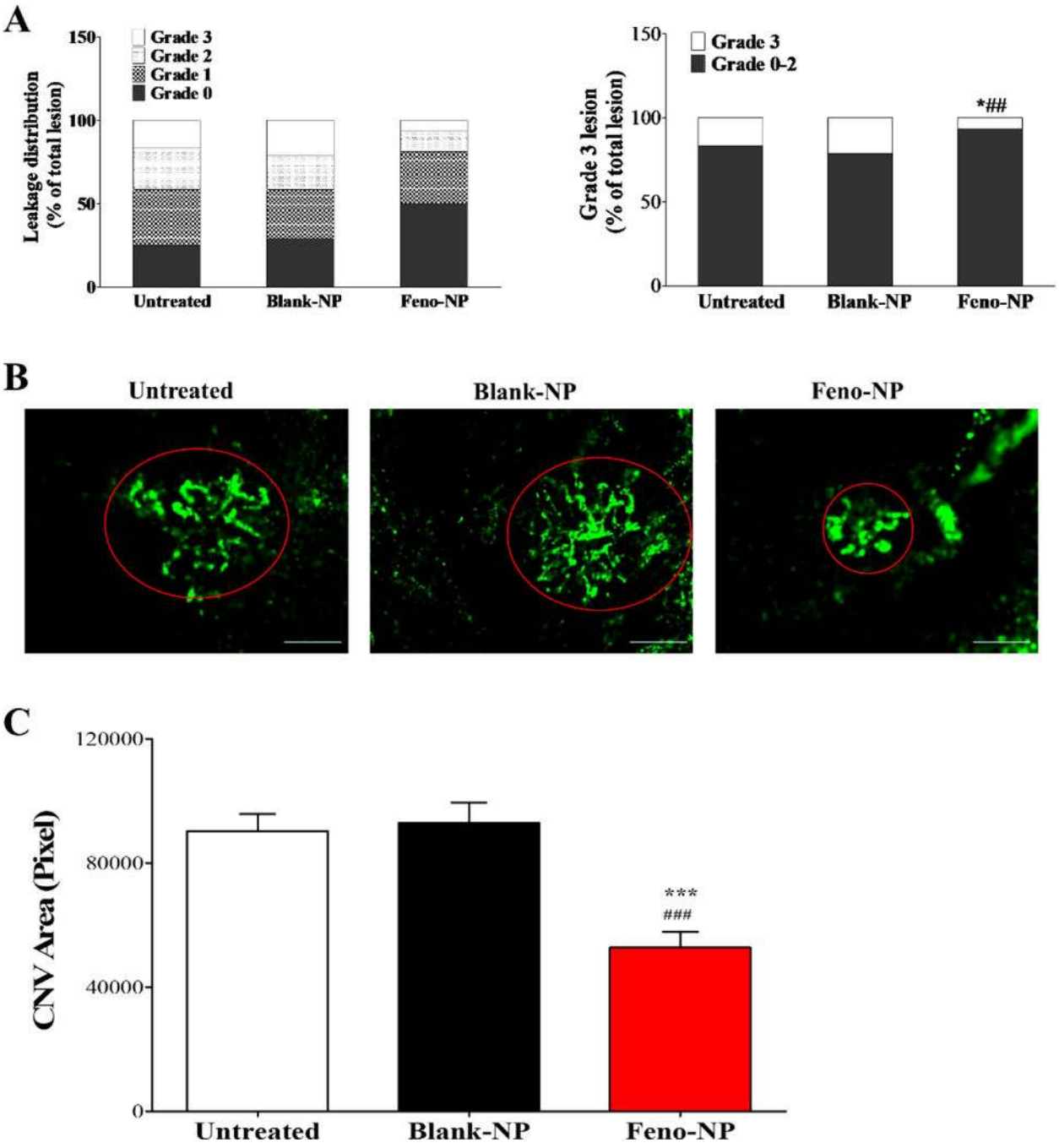

Figure 7.

Effect of Feno-NP on vascular leakage and the formation of CNV in laser-induced CNV rat model. Two weeks after Feno-NP treatment, vascular leakage was evaluated by FFA, and CNV evaluated by CNV area in choroidal flat mount. **(A)** Distribution of lesion grades and the incidence of Grade 3 lesions with FFA (n=6–12). Data were percentages (%) (n = 6–12) and analyzed by Chi-square test. * $P < 0.05$, versus untreated CNV rats. ## $P < 0.01$, versus Blank-NP treated CNV rats. **(B)** Representative images of choroidal flat mount. Red circles indicated CNV lesions. Scale bar: 50 μm. **(C)** Quantification data of CNV area on choroidal

flat mount. Mean ± SEM (n = 6–12). One-way ANOVA followed by Bonferroni post hoc test. *** $P < 0.001$, versus untreated CNV rats. ### $P < 0.001$, versus Blank-NP treated CNV rats.

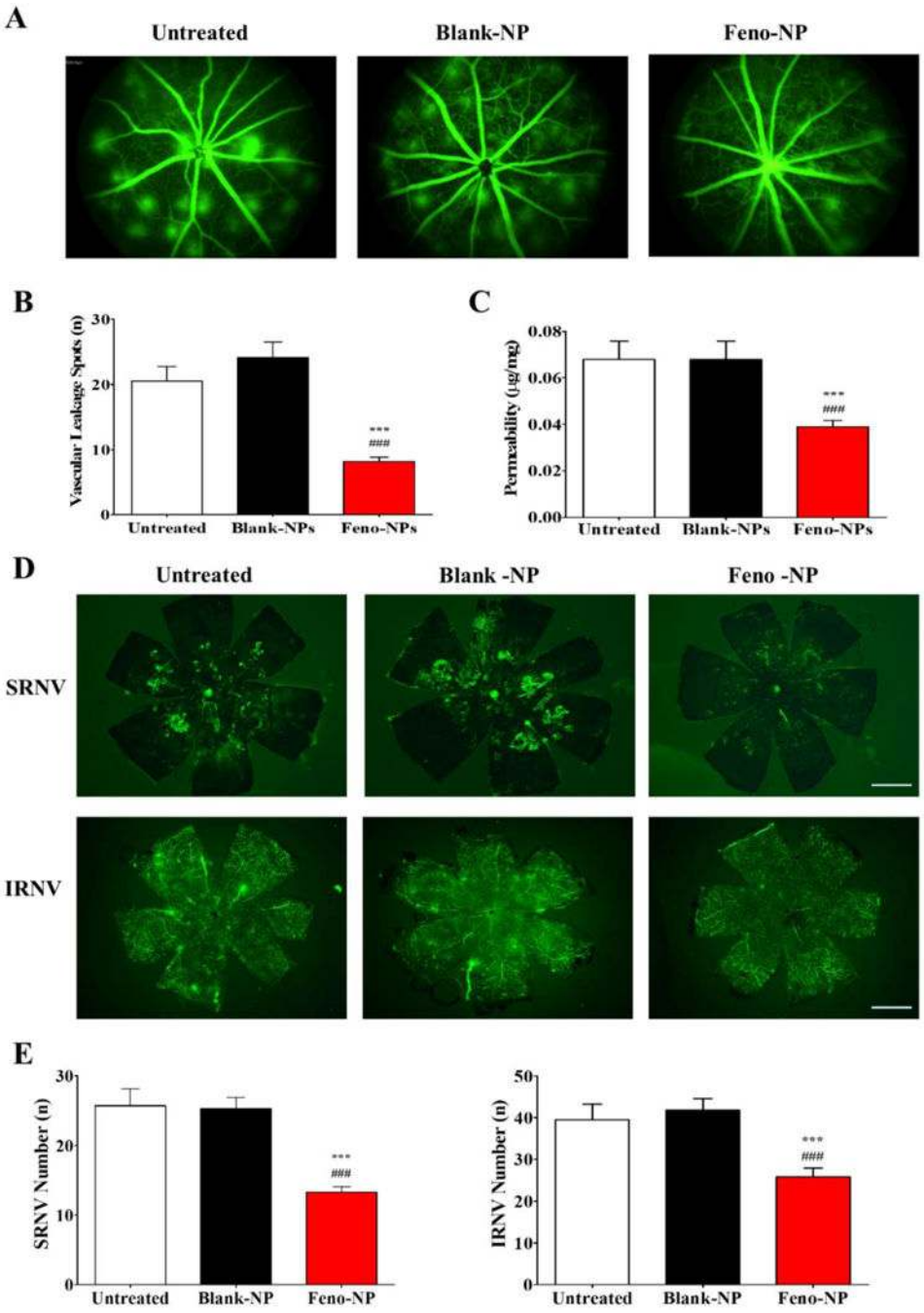

Figure 8.

Effect of Feno-NP on vascular leakage measured with FFA and vascular permeability, formation of SRNV and IRNV evaluated by neovascular tufts in flat-mounted choroid and retina in *Vldlr*$^{-/-}$ mice one month after Feno-NP treatment. **(A)** Representative images of FFA. **(B)** Numbers of leakage spots in FFA. **(C)** Quantification of retinal vascular permeability. **(D)** Representative images of SRNV and IRNV in FFA. Scale bar: 1,000 μm. **(E)** Quantification of SRNV and IRNV in flat mounted choroid and retina. Mean ± SEM (n

= 8–16. One-way ANOVA followed by Bonferroni post hoc test. *** P < 0.001, versus untreated *Vldlr*$^{-/-}$ mice. ### P < 0.001, versus Blank-NP treated *Vldlr*$^{-/-}$ mice.

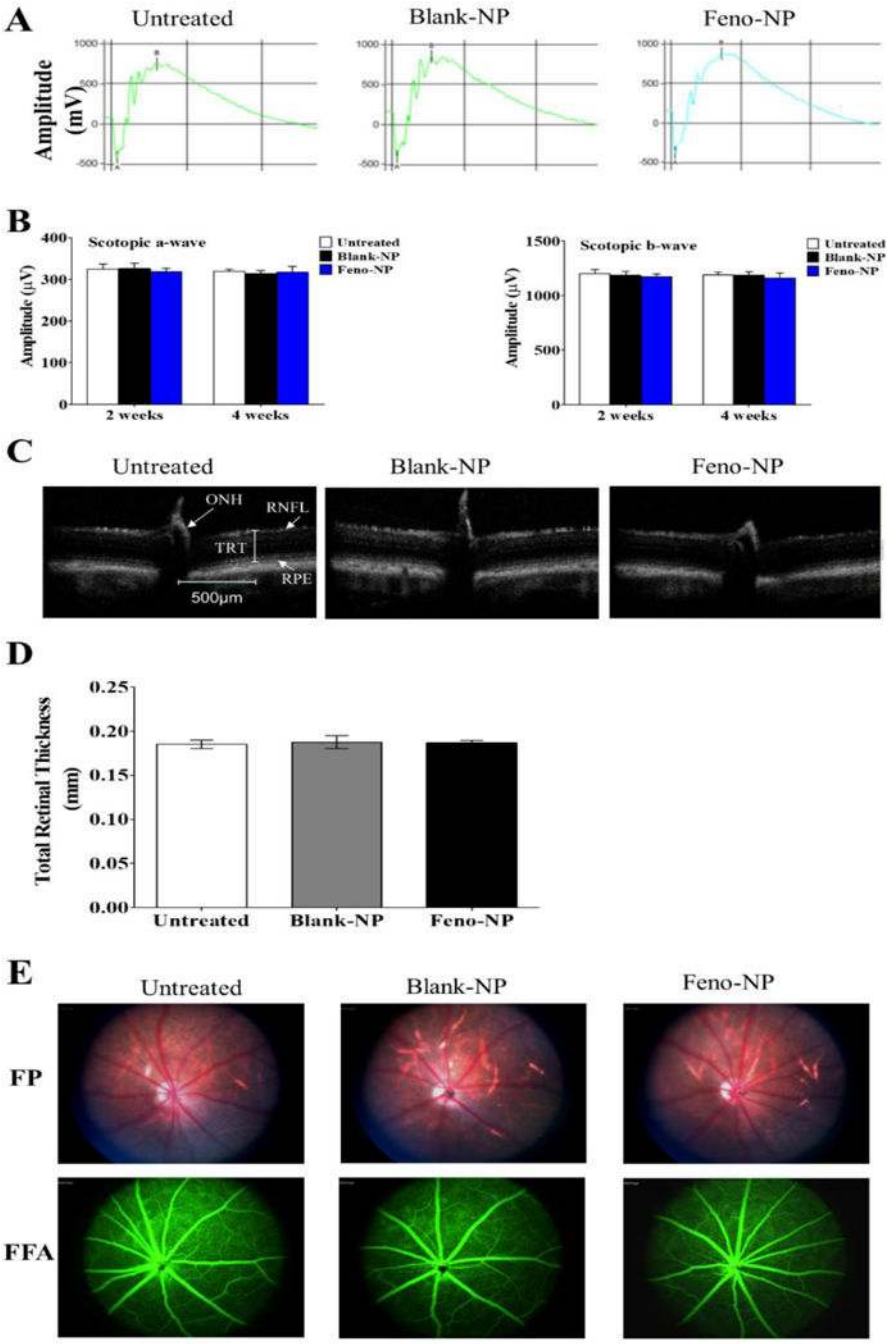

Figure 9.

Feno-NP or Blank-NP has no detectable toxicities to retinal function measured with ERG and morphology with FP, OCT and FFA in normal rats. **(A)** Representative waveforms of ERG. **(B)** Quantification of ERG. **(C)** Representative images of OCT. **(D)** Quantification of total retinal thickness in OCT. **(E)** Representative images of FP and FFA. Mean ± SEM (n = 8–16). TRT: total retinal thicknesses; RPE: retinal pigment epithelial layer; RNFL: retinal nerve fiber layer; ONH: optic nerve head. One-way ANOVA followed by Bonferroni post

hoc test. No statistically significant difference was found among untreated normal rats, Blank-NP treated normal rats and Feno-NP treated normal rats.

Table 1.

Evaluation of fluorescein leakage in CNV rats (grade 0–3), modified from [20].

Clinical parameter	Grade			
	0	1	2	3
Leakage	None	Questionable	Leaky	Pathologically significant leaky
Hyperfluorescence intensity	Faint or speckled	No advancing increase	Increase	Increase
Hyperfluorescence size	None	No advancing increase	Not significant increase, no definite leakage	Increase with definite leakage

Table 2.

Physicochemical Properties of NP

Polymer	Particle size (nm)	PDI	ζ-potential (mV)	Drug loading (wt. %)	EE (%)
PLGA 5kDa	224 ± 12	0.03 ± 0.02	−6 ± 4	1.1	6.6
PLGA 18kDa	250 ± 12	0.03 ± 0.01	−1.5 ± 0.5	4	24
PLGA 34kDa	265 ± 10	0.03 ± 0.01	−1.2 ± 0.1	6	36
PLGA 54kDa	252 ± 4	0.05 ± 0.03	−1 ± 0.2	7.9	47